https://doi.org/10.5194/essd-2023-59
Preprint. Discussion started: 28 March 2023

Open Access Earth System Science Data Discussions

Atmospheric and surface observations during the Saint John River Experiment on Cold Season Storms (SAJESS)

Hadleigh D. Thompson[1], Julie M. Thériault[1], Stephen J. Déry[2], Ronald E. Stewart[3], Dominique Boisvert[1], Lisa Rickard[2], Nicolas R. Leroux[1], Matteo Colli[5], Vincent Vionnet[4]

[1]Department of Earth and Atmospheric Sciences, Centre ESCER, Université du Québec à Montréal, Montréal, Quebec, H3C 3P8, Canada
[2]Department of Geography, Earth and Environmental Sciences and Natural Resources and Environmental Studies Program, University of Northern British Columbia, Prince George, British Columbia, V2N 4Z9, Canada
[3]Department of Environment and Geography, University of Manitoba, Winnipeg, Manitoba, R3T 2N2, Canada
[4] Meteorological Research Division, Environment and Climate Change Canada, Dorval, Quebec, H9P 1J3, Canada
[5]Artys Srl, Piazza della Vittoria, 9/3, 16121 Genova, Italy

Correspondence to: Julie M. Thériault (theriault.julie@uqam.ca)

Running title

Data from the Saint John River Experiment on Cold Season Storms (SAJESS)

https://doi.org/10.5194/essd-2023-59
Preprint. Discussion started: 28 March 2023

Open Access Earth System Science Data Discussions

Abstract. The amount and phase of cold season precipitation accumulating in the upper Saint John River basin are critical factors in determining spring runoff, ice-jams, and flooding in downstream communities. To study the impact of winter and spring storms on the snowpack in the upper Saint John River (SJR) basin, the Saint John River Experiment on Cold Season Storms (SAJESS) utilized meteorological instrumentation, upper air soundings, human observations, and hydrometeor macrophotography during winter/spring 2020-21. Here, we provide an overview of the SAJESS study area, field campaign, and existing data networks surrounding the upper SJR basin. Initially, meteorological instrumentation was co-located with an Environment and Climate Change Canada station near Edmundston, New Brunswick, in early December 2020. This was followed by an intensive observation period that involved manual observations, upper-air soundings, a multi-angle snowflake camera, macrophotography of solid hydrometeors, and advanced automated instrumentation throughout March and April 2021. The resulting datasets include optical disdrometer size and velocity distributions of hydrometeors, micro rain radar output, near-surface meteorological observations, and wind speed, temperature, pressure and precipitation amounts from a K63 Hotplate precipitation gauge, the first one operating in Canada. These data are publicly available from the Federated Research Data Repository at https://doi.org/10.20383/103.0591 (Thompson et al., 2022). We also include a synopsis of the data management plan and data processing, and a brief assessment of the rewards and challenges of utilizing community volunteers for hydro-meteorological citizen science.

https://doi.org/10.5194/essd-2023-59
Preprint. Discussion started: 28 March 2023

Open Access Earth System Science Data Discussions

1 Introduction

The Saint John River Experiment on Cold Season Storms (SAJESS) focused on cold region processes related to winter and spring storms over the transboundary upper Saint John River basin, located on the border of Maine (ME) and the provinces of Quebec (QC) and New Brunswick (NB). The Saint John River, known as the Wolastoq by local Indigenous communities, is 673 km long and drops 480 m in elevation from its source at the Little John River (ME) down to the Bay of Fundy (Fig. 1). It covers 55,000 km^2, with 36% located in the U.S., although, here we define the upper Saint John River basin as the area that drains into the Saint John River above Grand Falls, NB. Economically important to the region, the river provides flow for five hydroelectric facilities with development being overseen by the International Joint Commission (Kenny & Secord, 2010).

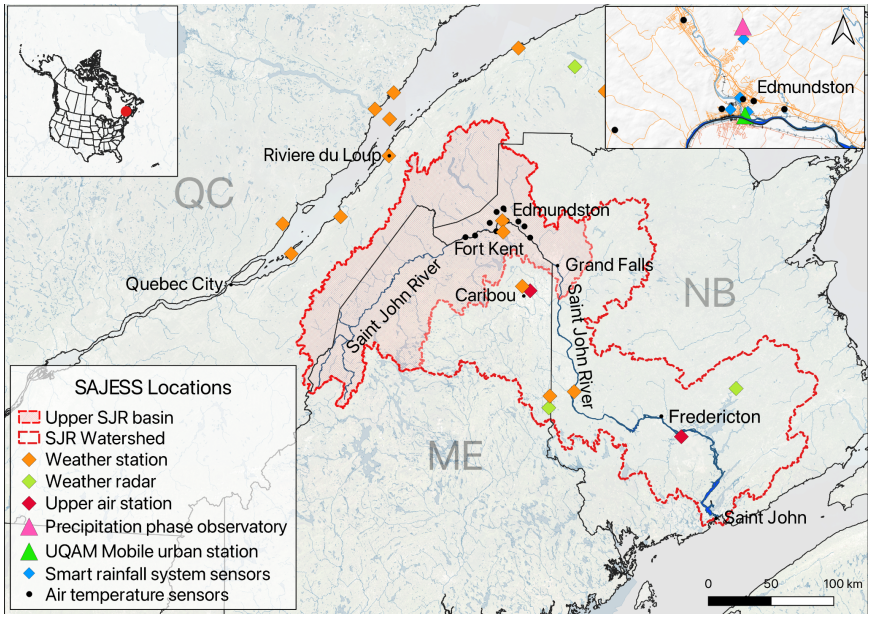

Figure 1: The Upper Saint John River Basin (shaded red), straddling the borders of Quebec (QC), Maine (ME, US) and New Brunswick (NB) is a sub-basin of the Saint John River Basin (red line). The Environment and Climate Change Canada (ECCC) and US National Weather Service (NWS) weather stations, the upper air stations, SAJESS-supplied CoCoRaHS stations (black circles), the Precipitation Phase Observatory/Fixed Station (pink triangle) and the UQAM Mobile urban station/Must Trailer (green triangle) are shown.

A concern of emergency managers along the Saint John River is the risk of catastrophic flooding when spring rain coincides with relatively high temperatures, creating significant snow melt. Such flooding events occurred in 2008, 2018, and again in 2019, and were in the annual top 10 Canadian weather disasters identified by

https://doi.org/10.5194/essd-2023-59
Preprint. Discussion started: 28 March 2023

Environment and Climate Change Canada (ECCC) (ECCC, 2017, 2019, 2020). Although this sub-catchment covers an area of 22,600 km^2, the majority of research focusing on the Saint John River does so by examining the lower reaches and associated lakes, wetlands, and tidal estuaries. There is therefore a paucity of both hydrological knowledge of the upper basin, as noted by Budhathoki et al. (2022), and meteorological stations (only two within the upper SJR basin) (also see Fortin and Dubreuil, 2020). Previous studies encompassing the Saint John River Basin have focused on flooding (Newton & Burrell, 2016), including rain-on-snow events (Buttle et al., 2016), and the analysis and modeling of ice jams that may increase in frequency in future climate scenarios (Beltaos et al. 2003). Despite these hazards, no studies of storms and precipitation and their impact on snowpack evolution have been conducted in this region.

The objective of this paper is to describe the data collected during SAJESS. Meteorological and precipitation data were collected at a fixed station from 1 December 2020 until 30 April 2021, and an intensive observational period (IOP) that took place from 8 March to 30 April 2021.

2 Site Descriptions

2.1 Overview

To observe the spatial and temporal variability in precipitation amount and phase across the study area, a broad range of techniques was employed: first, a semi-permanent 'Precipitation Phase Observatory' was installed to record meteorological data from December 2020 to April 2021. This site became known as the 'Fixed Station' and was co-located with the permanent ECCC station, north of Edmundston (Fig. 1). Second, the Mobile Urban Station (MUST), a modified enclosed trailer provided by the Université du Québec à Montréal (UQAM), was situated at the confluence of the Madawaska and Saint John rivers for the IOP during April and May 2021. The MUST was located on property provided by the City of Edmundston and was used as a base for graduate students and volunteers to record manual observations, capture macrophotography images of hydrometeors, and release sounding balloons for upper air observations. Finally, community volunteers were engaged by providing locations for either a satellite dish associated with the Smart Rainfall System (SRS) array (Coli et al., 2019), or a precipitation gauge and snow board for the Community Collaborative Rain, Hail, and Snow Network (CoCoRaHS) (Cifelli et al., 2005). Furthermore, up to 10 grade 6 classes (11-12 years old) from local elementary schools also enrolled as CoCoRaHS observers.

https://doi.org/10.5194/essd-2023-59
Preprint. Discussion started: 28 March 2023

2.2 Precipitation Phase Observatory

The Precipitation Phase Observatory (henceforth, the Fixed Station) encompassed a semi-permanent array of meteorological instruments that were installed ~100 m from the Edmundston ECCC station on 30 November 2020 (Table 1, Figs. 1 and 2). The site was situated at the southern end of an area of open grassland in a broad valley, 152 m above sea level (ASL). The valley is 120-200 m wide by 1 km long, oriented north-south, and bordered by coniferous forest. The 14-ha site acts as the municipal aquifer resupply and was provided by the city of Edmundston for the installation. We provide specific location details in Table 1. This site was chosen to allow for the SAJESS datasets to be supplemented with records from the nearby ECCC station, notably precipitation amounts from the shielded weighing precipitation gauge and 10-m wind speed and direction from the ECCC mast. Additionally, the open field provided an opportunity to install an Infrared Gas Analyzer and Sonic anemometer (IRGASON) to estimate surface turbulent fluxes and compute surface energy balances (Table 2) during the IOP (see Section 2.2).

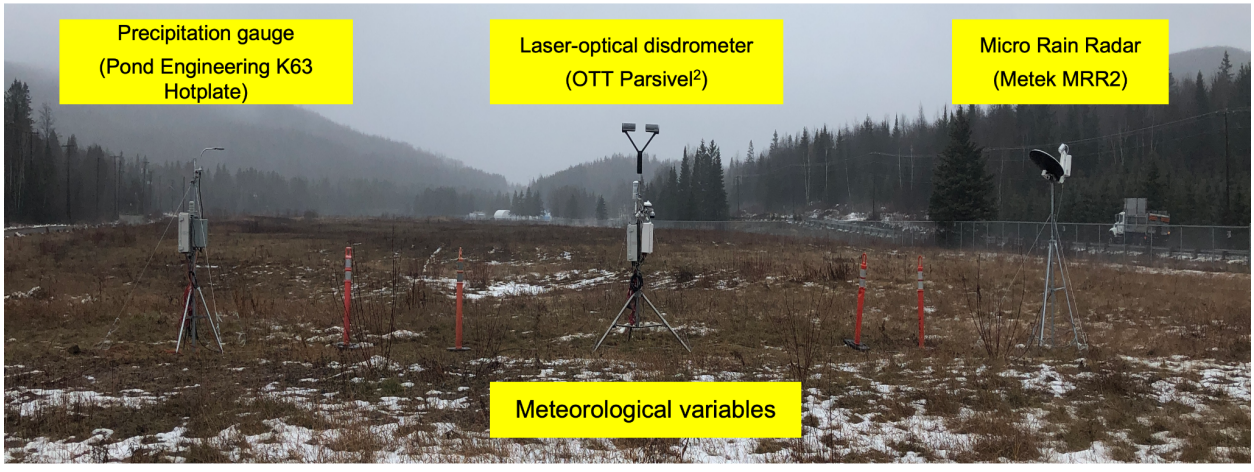

Figure 2: The Precipitation Phase Observatory instrumentation, image taken looking north. From left-to-right: The K63 Hotplate, a laser-optical disdrometer installed upon the meteorological tripod, and the Micro Rain Radar. This station was also to be known as the 'Fixed Station'. Picture taken 1 December 2020.

The identification of precipitation phase was achieved at the Fixed Station by the installation of a K63 Hotplate Precipitation Gauge (henceforth, hotplate) to measure precipitation rate and amount, a laser-optical disdrometer to discern particle type and record particle size and fall speed, and a vertically pointing micro rain radar (MRR) to provide information on the atmospheric conditions aloft (see Section 3 and Table 2). Aside from periods of

https://doi.org/10.5194/essd-2023-59
Preprint. Discussion started: 28 March 2023

missing data (~5%), the Fixed Station dataset, excluding the Flux Tripod (see Section 3.1.2), spans 1 December 2020 – 30 April 2021.

2.3 Intensive observation period

Due to limitations at the Fixed Station (e.g., no fuel or generator use), a separate IOP site was established so that the Mobile Urban Weather Station Trailer (MUST) and instruments could frequently be visited by observers (Fig. 1). The 6′ × 12′ enclosed trailer was equipped with heating, AC power, helium cylinders, and instrument storage; it was parked on a fenced parcel of land on the north bank of the Saint John River and the east bank of the mouth of the Madawaska River, 143 m ASL. Although the 3.3-ha site is dominated by the Edmundston wastewater ponds, there was sufficient space for the MUST Trailer and instrumentation to be placed along the northern edge of the site (Figure 4).

https://doi.org/10.5194/essd-2023-59
Preprint. Discussion started: 28 March 2023

Open Access Earth System Science Data Discussions

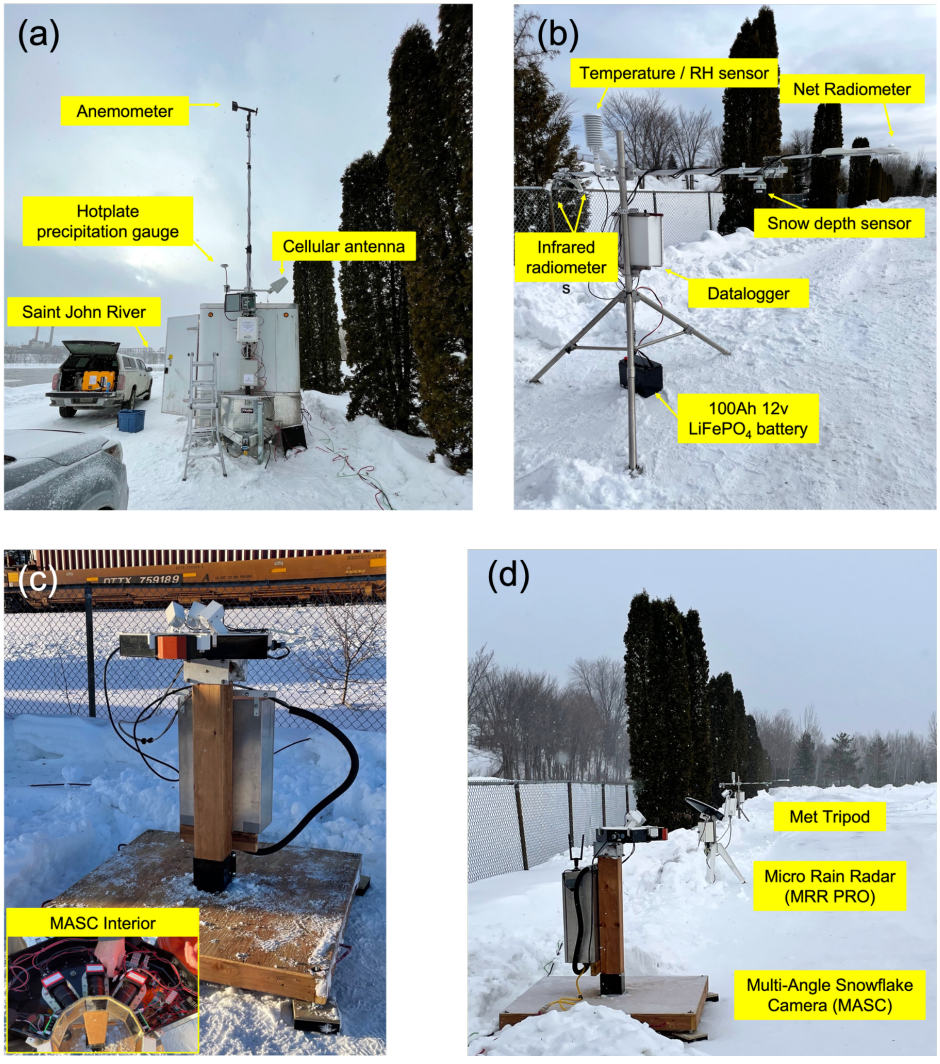

Figure 3: Instruments and sensors co-located with the Mobile Urban Station (MUST) trailer. (a) The MUST trailer with extended 10 m mast, anemometer, and K63 Hotplate (a), (b) the meteorological tripod, (c) the Multi-Angle Snow Camera (MASC) with a top-down view of the internal components and three high-speed cameras, and (d) the MASC, MRR Pro, and meteorological tripod lined along the access road to the water treatment lagoon. Pictures taken 3 March 2021.

The proximity of the instruments to the open ponds, nearby railway, and urban environment, resulted in the focus on observations, rather than instrumentation, at this location. We therefore stationed equipment that required regular attention or manual operation, such as the multi-angle snowflake camera (MASC) (Figure 4c) and

https://doi.org/10.5194/essd-2023-59
Preprint. Discussion started: 28 March 2023

macrophotography equipment (not shown). Manual observations and macrophotography (see Section 3.2) were conducted at the site from 1 March 2021 – 27 April 2021.

2.3 Smart Rainfall System (SRS)

The Smart Rainfall System (SRS) was installed at several sites in the Edmundston area to capture the spatial variability of precipitation by exploiting the satellite-to-earth links technology (Colli et al., 2019). Some locations were also chosen to provide measurements upstream and downstream of Edmundston. The SRS system uses a standard parabolic dish to receive satellite telecommunication broadcasting signals and an algorithm converts the signal attenuation to precipitation rate (section 3.4). Locations with parabolic dishes that were already installed by community volunteers for telecommunication purposes, but not being used during the experiment period, were selected. The specific locations are shown Fig. 1.

2.4 Community involvement (CoCoRaHS)

While the CoCoRaHS network provides a broad array of precipitation measurements across North America (Reges et al., 2016), there were few CoCoRaHS observer sites in the SAJESS study region. With assistance from CoCoRaHS Canada (Colorado Climate Center, 2017), SAJESS students and staff facilitated the distribution of equipment and training to a total of 22 new CoCoRaHS stations, including 11 elementary schools, during the 2020-2021 winter season. CoCoRaHS site metadata available to the public can be found at https://cocorahs.org/Stations/ListStations.aspx.

3. Field instruments and manual observations

3.1 Instrumentation

The main consideration when deploying instruments to SAJESS was how to measure the amount, phase, and type of precipitation that occur during the winter and spring seasons. Particular attention was paid to gathering data throughout as much of the tropospheric column as possible.

Here we provide an overview of the instrumentation used during SAJESS. Sensor details, parameters, and units are included in Tables 2 and 3. Details of each sensor are also provided with the dataset.

https://doi.org/10.5194/essd-2023-59
Preprint. Discussion started: 28 March 2023

147 **3.1.1 Meteorological tripod**

148 Standard meteorological variables were measured at each of the two main sites. Common parameters for each site
149 were 2-m air temperature and relative humidity, 4-way net radiation (upwelling and downwelling long-wave and
150 short-wave radiation, LW↑, LW↓, SW↑, and SW↓), surface temperature, and snow depth. Measurements at the
151 Fixed Station also included soil surface temperature and moisture content. Snow at the Fixed Station remained
152 undisturbed for the winter and total snow depth was recorded continuously for December 2020 – April 2021. Due
153 to disturbance of the snowpack surrounding the MUST Trailer by foot traffic and installation of other instruments,
154 a 30 cm × 30 cm white snow board was placed underneath the snow depth sensor and cleared after each significant
155 snowfall event. On each met tripod, the snow depth sensor was installed on the south end of the tripod cross arm
156 so that the legs of the tripod would not be within ~1 m diameter cone of detection. For surface temperature, two
157 infrared radiometers (IRRs, henceforth IRR 1 and IRR 2) were mounted to the north end of the cross arm of each
158 met tripod and angled away ~ 30 degrees. At the Fixed Station, IR 1 faced slightly west, while IR 2 faced slightly
159 east. At the MUST Trailer site these were reversed. The net radiometer and snow depth sensors were mounted on
160 the south end of each cross arms.

161 **3.1.2 Flux tripod**

162 An Open-path Eddy Covariance system was installed at the Fixed Station for the IOP from 5 March 2021 to 30
163 April 2021. The integrated Infrared Gas analyzer and Sonic Anemometer (IRGASON), temperature/RH probe,
164 net radiometer, infrared radiometer, soil probes, and heat flux plates were installed following the prescribed
165 methods found in Campbell Scientific (2022a), with the IRGASON sensor facing north into the prevailing wind.
166 Winds (in 3-D), air temperature, ambient pressure, and CO_2 and H_2O densities were captured at 10 Hz resolution
167 and averaged over 30 minutes to calculate turbulent fluxes and energy closure balances (Campbell Scientific,
168 2022b). The dataset also includes diagnostic data, data quality values, and coefficients used for the eddy-
169 covariance calculations during each 30-min period so the raw time series data can also be post-processed using a
170 variety of software (US Department of Energy, 2022).
171

https://doi.org/10.5194/essd-2023-59
Preprint. Discussion started: 28 March 2023

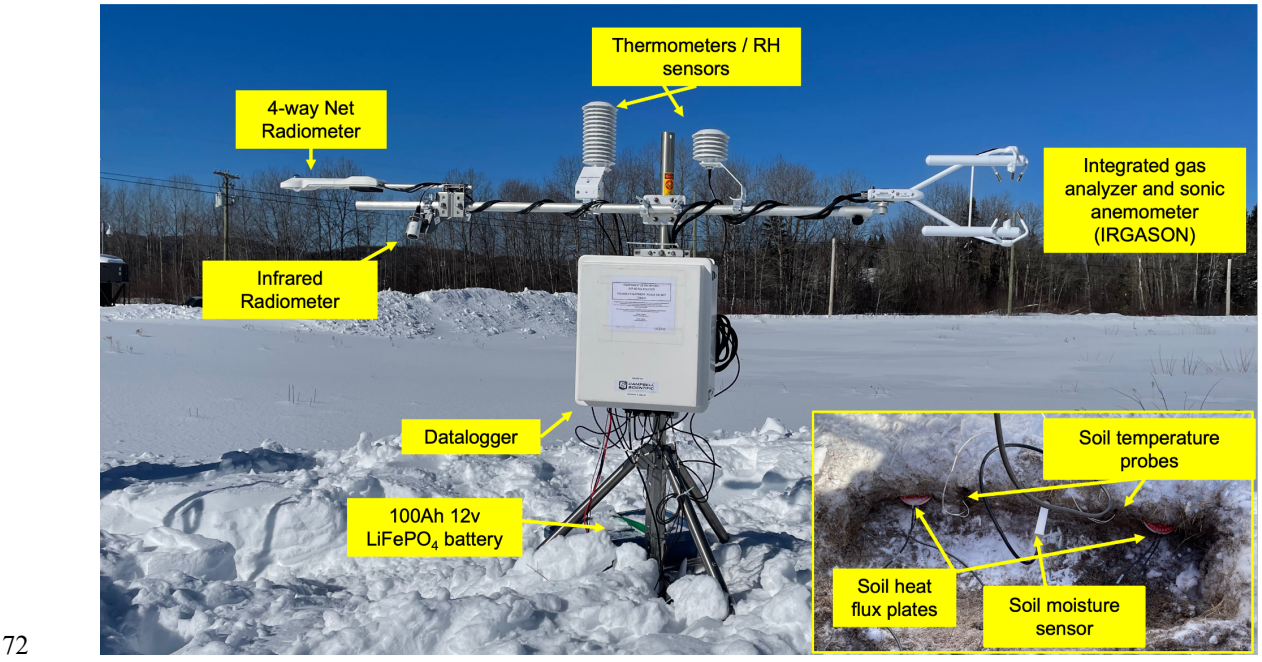

Figure 4: The Fixed Station flux tripod. An open-path eddy-covariance system consisting of an Infrared Gas Analyser and Sonic Anemometer (IRGASON), soil temperature probes, a soil moisture sensor, a net radiometer, an infrared radiometer, and temperature/RH sensors. This tripod was installed for the melt period from 5 March to 30 April 2021. Picture taken 5 March 2021.

3.1.3 Hotplate precipitation gauge

A hotplate precipitation gauge (henceforth, hotplate) was installed at the eastern end of the Fixed Station instrument array (Fig. 3) (Rasmussen et al., 2011; Thériault et al., 2021b). As outlined by Cauteruccio et al. (2021), the hotplate was tested during the World Meteorological Organization's Solid Precipitation Intercomparison Experiment (SPICE) (Nitu et al. 2018), and the Global Precipitation Measurement Cold Season Precipitation Experiment (GCPEX) (Skofronick-Jackson et al. 2015). SAJESS was the first time in Canada that the Pond Engineering version of the hotplate was used in a field campaign. A second one of this type of hotplate was installed for the IOP on the MUST Trailer mast and is detailed in Section 3.1.7.

3.1.4 Disdrometer

A laser-optical disdrometer was deployed at the Fixed Station for the duration of the field campaign on the same tripod as the standard meteorological instruments, at 2.8 m AGL (Fig. 3), to measure the size and speed of falling hydrometeors and allow the classification of hydrometeor type (Hauser et al., 1984; Löffler-Mang and Joss, 2000;

https://doi.org/10.5194/essd-2023-59
Preprint. Discussion started: 28 March 2023

189 Thériault et al., 2021a). Disdrometer data include precipitation intensity (mm h^{-1}), number of detected particles,
190 various national standard present weather codes, and a 32 × 32 matrix of fall speed and particle diameter bins,
191 every 60 s.

192 **3.1.5 Micro Rain Radar**

193 A micro rain radar (MRR) at each of the primary sites was used during SAJESS to vertically profile hydrometeor
194 reflectivity and Doppler velocity (Tokay et al., 2009; Souverijns et al., 2017). A METEK MRR-2 was installed at
195 the Fixed Station, 2.6 m AGL, at the western end of the instrument array (Fig. 3). Raw data from the MRR-2 were
196 post-processed using the IMProToo algorithm from Mahn and Kollias (2012), as outlined in Thériault et al.
197 (2021a). A MRR-Pro was installed at 1.3 m AGL at the MUST Trailer (Fig. 4d). Both radar units used built-in
198 dish heating to eliminate snow and ice build-up during precipitation events.

199 **3.1.6 Multi-Angle Snowflake Camera**

200 A multi-angle snowflake camera (MASC) was installed at the MUST Trailer (Fig. 4c and d), on a wooden stand
201 ~1.4 m above the ground, for the majority of the IOP (5 March 2021 – 27 April 2021). Accumulating snow around
202 the base of the stand was removed by students to prevent the re-suspension of previously captured particles (Fitch
203 et al., 2021; Schaer et al., 2020). The MASC consists of three high-speed cameras housed in a single enclosure
204 that capture images simultaneously when particles are detected within a ring-shaped viewing area (Fig. 4c inset).
205 First introduced by Garrent et al. (2012), MASCs have been deployed in Antarctica (Praz et al., 2017), the
206 Colorado Rockies (Hicks & Notaros, 2019), and Alaska (Fitch et al., 2020), and a suite of machine learning
207 algorithms have been developed from these campaigns to automate the post-processing of the dataset.

208 **3.1.7 MUST Trailer mast**

209 A telescopic pneumatic 10-m mast attached to the MUST trailer supported an anemometer and wind vane (at 10
210 m), a hotplate precipitation gauge at 3.5 m, and the antenna for upper air observations (see Section 3.3) (Figure
211 4a). Due to air leakage, the mast did not always maintain its full extension and therefore required re-extending at
212 times, causing wind speed and direction measurements to not always be reliable. These observations are still
213 useful, however, for identifying periods of relatively high wind speeds that may have led to snow re-suspension
214 with the subsequent blowing snow being captured by the MASC, while observers were not on site to record such
215 episodes.

https://doi.org/10.5194/essd-2023-59
Preprint. Discussion started: 28 March 2023

3.2 Macrophotography, manual observations, and timelapse images

Observers were present at the MUST Trailer during periods of precipitation to report weather conditions, and to obtain macrophotographs of solid hydrometeors (Gibson and Stewart, 2007; Joe et al., 2014; Thériault et al., 2018; Lachapelle and Thériault, 2021a). Observations of sky condition, cloud type, and precipitation type (solid, liquid, or mixed), and images from a digital SLR camera fitted with a macro lens and ring flash, were taken every 10 min. This was especially important with respect to hydrometeor type during mixed phased precipitation around 0°C due to the potential for misdiagnosis by instrumentation and modeling. Other noted conditions were the occurrence of very light precipitation which can be missed by disdrometers, and the presence of blowing snow that could affect analysis of MASC data (Section 3.1.6). Hourly images of each site, including the surface conditions around the instruments, were captured by a time lapse camera.

3.3 Upper air observations

Atmospheric soundings using a portable sounding system were released prior to and during periods of precipitation. Soundings were timed to coincide with standard synoptic launch times (00 UTC, 12 UTC) and additional launches were attempted every three hours. A total of 52 balloons were launched from the MUST Trailer and 46 of those launches resulted in a complete sounding of the troposphere from which profiles of pressure, temperature, dew point and winds (speed and direction) can be produced.

3.4 Smart Rainfall System

SAJESS provided the opportunity to deploy an innovative environmental monitoring technique, the Smart Rainfall System (SRS), that has been developed by the University of Genoa, Genoa, Italy and currently distributed by Artys srl. The SRS produces estimations of liquid precipitation, in 1-min rainfall intensity, by processing the attenuation of the satellite microwave link (SML) signal emitted by commercial geosynchronous satellites for Digital Video Broadcasting (DVB-S) and received by common parabolic antennas (Colli et al., 2019). Estimating liquid precipitation using the SRS has been confirmed by several experimental initiatives (Giannetti et al., 2021). In contrast, snowfall intensity retrieval at centimeter wavelengths (the DVB-S signal is transmitted in the Ku frequency band) is more uncertain. It has been demonstrated that higher operating frequencies, and preferably dual-band systems, are needed to successfully retrieve solid precipitation (Falconi et al., 2018; Liao et al., 2016).

https://doi.org/10.5194/essd-2023-59
Preprint. Discussion started: 28 March 2023

The SAJESS experiment represents the first operational use of the SRS for monitoring the liquid content in cases of mixed precipitation and wet (melting) snow. The SRS system tested in Edmundston was composed of a set of distributed SML sensors, as described by Colli et al. (2019), connected to a central processing and analysis node to reconstruct the bi-dimensional rainfall field in real time.

3.5 CoCoRaHS sites

3.5.1 CoCoRaHS gauges and snowboards

Volunteers from the community contributed to SAJESS by recording meteorological measurements for the CoCoRaHS network (Cifelli et al., 2005). A typical CoCoRaHS station includes a manual precipitation gauge to measure liquid and solid precipitation, and a 40 cm × 40 cm white board for measuring snow depth. Daily measurements include the amount of precipitation, depth of snowfall, and snow water equivalent (SWE). Weekly measurements consist of total snow depth, and the total SWE. CoCoRaHS data can be found using the network's online database; stations associated with the project have *SaJESS* in the station name. In addition to the regular CoCoRaHS station equipment, some volunteers hosted dataloggers to record air temperature and relative humidity (see below).

3.5.2 Temperature sensors

HOBO MX2301A data loggers were distributed to 13 community volunteers (Fig. 1, Table 4). Installed approximately 2 m above the ground, the dataloggers measure air temperature and relative humidity every 5 minutes (Onset Computer Corporation, 2022). Data were retrieved from the HOBO devices via a Bluetooth smartphone app that reduced the need to handle the sensor.

4 Data description

4.1 Data processing and management

Here we provide a short summary of the data processing and archiving strategies. Full details on all data, including specifications of the instruments used, can be found in the readme files uploaded to the FRDR repository.

Firstly, all instrumentation, camera equipment, observer notes, and computers were set to UTC date and time. Instruments that produce relatively low-volume text-based data such as the disdrometer, meteorological tripods,

https://doi.org/10.5194/essd-2023-59
Preprint. Discussion started: 28 March 2023

hotplate precipitation gauge, and temperature sensors, have been processed by concatenating smaller files together to create monthly files. Missing timestamps have been added to ensure every file contains timesteps for each minute of the month. All missing data points have been filled with NANs and no interpolation of missing data points has been attempted for the data uploaded to the FRDR repository. For standard meteorological variables such as temperature, humidity, snow depth, and radiation measurements, values have been quality checked to ensure they fall within the operating range of each instrument, with values outside of these ranges being set to NAN.

Raw radar data (.raw files) from the Fixed Station radar have been processed into daily NetCDF (.nc) format using the algorithm detailed by Maahn & Kollias (2012). Both .raw and .nc files have been included in this dataset. Hourly data from the MUST Trailer radar (MRR Pro) have been archived as .nc files as these data are produced in-situ by the instruments embedded processor (METEK, 2017).

Photographic images have not been altered or cropped and are uploaded as .png files for the MASC and macrophotography, or .jpg files for the timelapse cameras. Manual observations recorded in spreadsheets have been archived as comma separated value (.csv) files. Upper air observations are saved as one file per sounding, in tabular-delimited files, indexed by UTC date and time at a temporal resolution of 1 second.

In most instances, files have been identified using a specific naming convention using abbreviations for the project (SAJESS, SJ), each site (Fixed Station, FS; MUST Trailer MT), and each instrument (see Tables 2 and 3). For example, data from the disdrometer at the Fixed Station for the month of January 2021 are contained in the file: SJ_FS_DIS_MAS_202112.txt. (The abbreviation MAS stands for master and is used by the field staff to identify data that have been assembled ready for upload to the repository). MASC images do not follow this naming convention as the software used with the instrument provides a detailed filename with respect to the snowflake number and timestamp of the image.

4.2 Data validity

While not exhaustive, we list below known issues and attempts to-date at validating data from the SAJESS instruments and observations. We invite users to contact us for further information as several projects using SAJESS data are ongoing.

https://doi.org/10.5194/essd-2023-59
Preprint. Discussion started: 28 March 2023

298 **4.2.1 Met Tripod**

299 To our knowledge the only instrument to suffer from a systematic error was the HMP155A temperature and
300 humidity probe located on the meteorological tripod at the Fixed Station. Incomplete grounding at the datalogger,
301 and the subsequent datalogger program, resulted in a bias of ~ -2.32°C when compared to temperature data from
302 the ECCC station (Fig. 5). Due to the uniform pattern of the bias resulting in a low RMSE, these data have been
303 retained in the dataset and are available for use. Correction of these data by +2.32°C in on-going snow modeling
304 analyses indicate these data are still useful if post-processed accordingly. Post-deployment testing indicates that
305 this bias is not present in the temperature data from the MUST Trailer met tripod.
306
307 While data from the hotplate precipitation gauge include air temperature and humidity that align well with the
308 ECCC station (i.e., do not require bias correction), these data have significantly more noise than data from the
309 meteorological tripod sensor.
310

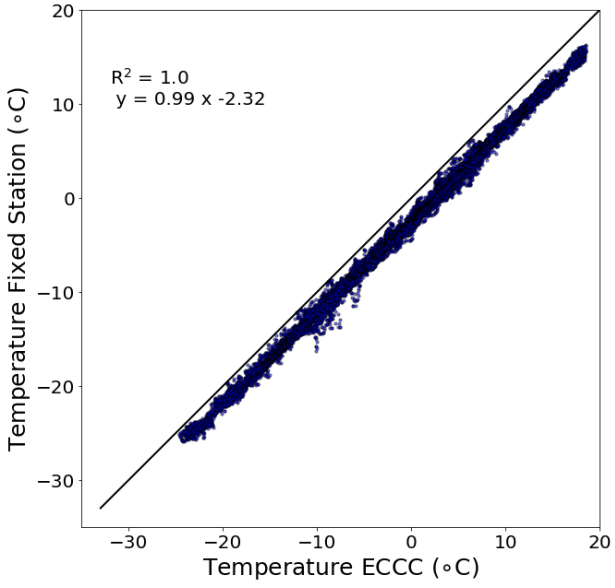

311
312 Figure 5: SAJESS Fixed Station and ECCC temperature data. Comparison of 1-minute temperature data (63149
313 recordings) from the Fixed Station temperature probe and the mean of the three ECCC temperature thermistor
314 readings. The Fixed Station HMP155 has a -2.32 °C bias due to the method of wiring and data recording.
315

https://doi.org/10.5194/essd-2023-59
Preprint. Discussion started: 28 March 2023

316 Analysis of the IRR surface temperature data indicates that shading from the tripod and datalogger enclosure may
317 have affected these measurements. When snow was present, the side with a shaded field of view (west in AM,
318 east in PM) measured warmer conditions (up to ~2°C) than on the unshaded side. Once snow cover was absent,
319 the trend was reversed so that the shaded side is cooler (up to ~6°C). This diurnal pattern of temperature difference
320 between the two sensors existed at both SAJESS locations, so we caution against the averaging of both sensors
321 without taking these differences into account. Although the 4-way net radiometer provides LW↑, we found
322 similar results to Domine et al. (2021) where RMSE between the net-radiometer and the IRRs was best reduced
323 using an unphysical emissivity (ε) value of 1.028. This could indicate that direct comparison is difficult due to the
324 difference in wavelength spectrum measured by the two instruments (Domine et al., 2021), yet the greater field
325 of view of the net radiometer may also be influential. Surface temperature data have not been corrected for surface
326 emissivity, and assume ε = 1 (Apogee Instruments Inc., 2022). The location of the IRRs should be installed on the
327 unshaded south end of the cross arm in future deployment.
328
329 Data from the SR50A on the Fixed Station meteorological tripod were within 10% of the same sensors used by
330 ECCC at the Edmundston station over the course of the 2020-21 winter. At both SAJESS sites, the 1-min
331 resolution caused noise in the snow depth data during periods of precipitation, which is greatly reduced using a
332 1-hour running mean. Data from the SR50A also include a 'quality number', which is detailed in the dataset
333 readme and can be used to filter snow depth data.
334
335 The 4-way net radiometers on each meteorological tripod were fitted with the heater/ventilation unit to reduce
336 errors associated with dew/frost on the sensor window. This unit, however, does not heat the sensor window(s)
337 sufficiently to remove snow or ice during or after precipitation, which is observed in the pyranometer data when
338 SW↑ is greater than SW↓, and correlated with precipitation events using the disdrometer and/or snow depth data.
339 This situation occurred on 13 days at the Fixed Station and five days at the MUST Trailer. For data analysis we
340 suggest using more advanced algorithms such as Lapo et al. (2015) to identify periods of snow accumulation,
341 which can then be corrected with other methods available in the literature (e.g., Sicart et al., 2006; Annandale et
342 al., 2002). Unlike Domine et al. (2021), no sustained periods of 0.0 W m^{-2} are observed in the LW↓ data, indicating
343 the continuous use of the ventilation unit was successful in preventing frost build-up.

https://doi.org/10.5194/essd-2023-59
Preprint. Discussion started: 28 March 2023


Open Access Earth System Science Data Discussions

344 **4.2.2 Flux tripod**

345 Users wishing to utilize data from the flux tripod can investigate variables provided in the Flux Notes (FN),
346 Campbell Scientific (CS), and AmeriFlux (AM) files. These include the number of H2O and CO2 samples per
347 averaging period, and a corresponding 'bad data' column. We observe that the maximum number of samples at
348 10 Hz for the 30-minute period (18,000 in total) did not reach a total of 19.5 hours during the March-April 2021
349 IOP. These occurrences correspond to periods of precipitation whereby we presume the IRGASON windows were
350 inhibited by rain/snow. On a finer scale, steady state integral turbulence characteristic (SSITC) tests were applied
351 to energy balance components for every 30-minute period (Foken et al., 2004). These can be found in the AM
352 files as variables named '_SSITC_TEST', and in the CS files as variables named '_QC'. Users should consult
353 Foken et al. (2004) for further information regarding these tests as further analysis is beyond the scope of the
354 paper. Data have not been gap-filled, removed, or replaced from the dataset.
355

https://doi.org/10.5194/essd-2023-59
Preprint. Discussion started: 28 March 2023

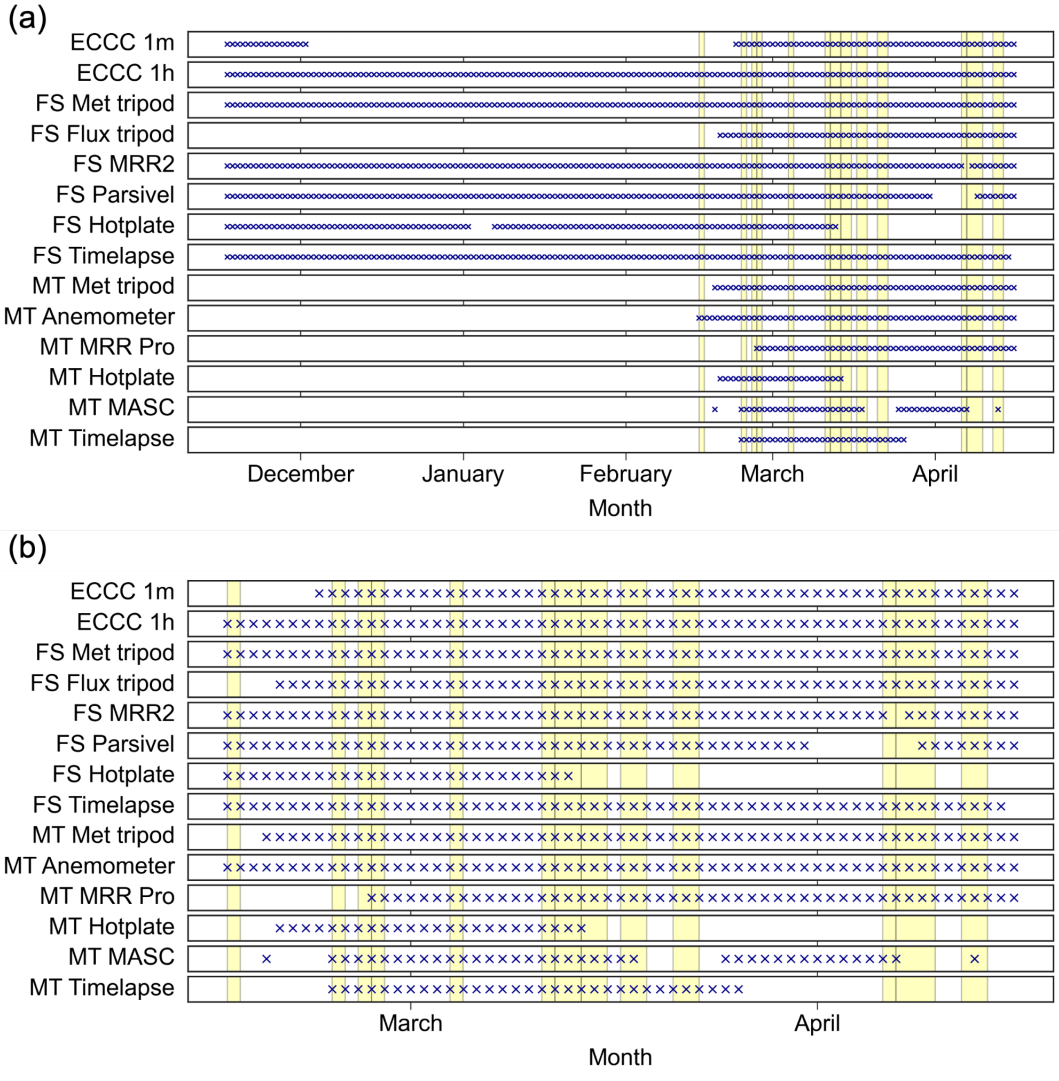

Figure 6: **Data availability (daily resolution). Operating periods for instrumentation for (a) the entire SAJESS field campaign, 1 December 2021 – 30 April 2021, and (b) during the intensive observation period, 1 March 2021 – 30 April 2021 (bottom). Data availability for the Environment and Climate Change Canada station in Edmundston is given for illustrative purposes only, as ECCC data are not included with this dataset. (FS stands for Fixed Station, and MT for MUST Trailer). Vertical yellow bands indicate periods of manual observations at the MUST Trailer during storm events by SAJESS volunteers and students.**

https://doi.org/10.5194/essd-2023-59
Preprint. Discussion started: 28 March 2023

363 **4.2.3 Hotplate**

364 Although the hotplate performed well when fully operational, a significant portion of the IOP was missed (28
365 March 2021 to 30 April 2021) due to faulty microprocessor settings on both hotplates (Fig 6). These have
366 subsequently been improved upon by the manufacturer, and further testing is underway. As described by
367 Rasmussen et al. (2011), hotplate precipitation rate accuracy is least assured during the onset and cessation of
368 precipitation, however, data from the hotplates include a 'Status' variable (#1, #2, or #3), that identifies these
369 periods. A full explanation is provided with the dataset readme. Precipitation data from the hotplate have not been
370 corrected for these under- or over-estimations.
371
372 Similar to Thériault et al. (2021b), we compared 30-minute cumulative sums of the hotplate 1-minute
373 accumulation for Dec 2020 – March 2021, with corrected GEONOR data (using Kochendorfer et al., 2017) from
374 the Edmundston ECCC station. These align well with the best results (reduced bias and RMSE) found for rain
375 (>2°C) and snow (<-2°C). Finally, hotplate T1 (1-minute average) precipitation data are more sensitive and
376 therefore better at reproducing higher precipitation rates than the T5 (5-minute average) data, resulting in a
377 positive bias up to ~1.5 mm h^{-1} (at 4-5 mm h^{-1}).
378
379 Due to processor issues, barometer data were not recorded by the hotplate environmental sensor at all 1- or 5-
380 minute intervals, however, valid readings do exist for each hour of the campaign. We recommend filtering
381 barometer data from both SAJESS sites by selecting the median value during each hour to represent the hourly
382 value. This method correlates well with ECCC station pressure reading (within 4 hPa) for the duration of the
383 campaign. Barometer readings represent raw station pressure and are not corrected for elevation.

384 **4.2.4 Disdrometer**

385 Although our primary use of Parsivel^2 disdrometer data concentrates on the diagnosis of hydrometeor phase and
386 type, other variables (e.g., METAR weather codes, Radar reflectivity, Kinetic energy) can be useful across
387 hydrometeorological disciplines. We include all variables with the dataset, however, at present we can only
388 comment on a preliminary analysis of the disdrometer-derived precipitation intensity. When compared to 30-
389 minute ECCC GEONOR and hotplate precipitation rates, timing and amounts from the disdrometer are generally
390 comparable, yet we observe the Parsivel^2 overestimates at high precipitation rates (>10 mm hr^{-1}), which is well
391 documented (e.g., Angulo-Martínez et al., 2018). Users wishing to utilize the drop size and fall speed distributions,
392 and subsequently retrieve an improved precipitation rate, can correct these data using Raupach and Berne (2015).

https://doi.org/10.5194/essd-2023-59
Preprint. Discussion started: 28 March 2023


Open Access Earth System Science Data Discussions

393 **4.2.5 Upper air observations**

394 Comparisons from four soundings from the MUST Trailer that aligned with either the 1200 UTC or 0000 UTC
395 balloon releases from Caribou (ME) were made for data from 18, 27, and 29 March 2021, with all four sounding
396 profiles displaying good agreement between the two sites. On some occasions, surface, and lower troposphere
397 (<700 hPa) temperatures at Edmundston were up to 5°C cooler than in Caribou, ~60 km to the northwest. The
398 SAJESS sounding data also correlate well with the surface observations of precipitation type and phase. We
399 recommend smoothing the 1 s sounding data using a low pass filter (e.g., 10 s running mean) to remove noise in
400 the temperature and dewpoint profiles.

401 **4.3 Examples of data and observations**

402 Here we provide examples of data from each of the two SAJESS sites to illustrate possible uses. While the total
403 SAJESS dataset is ~200 Gb, a ~1.1 Gb sample of data is available on the FRDR repository. This sample dataset
404 is based on the example given here for the MUST Trailer location, where a subset of data for 18 March 2021 is
405 displayed. Sample data have been made available for most instruments for the entire day (0000 – 2359 UTC), and
406 for the MASC, macrophotography images, and the MRRs for 1200 – 1300 UTC 18 March 2023 (to reduce file
407 size).

408 **4.3.1 Winter 2020-21**

409 Data covering winter 2020-21 through to spring 2021 is provided by the instruments at the Fixed Station (Fig. 7).
410 The SAJESS snow depth and precipitation data can also be supplemented with data from a weighing precipitation
411 gauge and triplicate snow depth sensors at the nearby ECCC station (not shown). Maximum snow depth measured
412 at the Fixed Station was 65 cm, with snowfall amounts comparing well in timing, yet slightly less in magnitude
413 (around 10%), than measured at the nearby ECCC station (not shown).
414

https://doi.org/10.5194/essd-2023-59
Preprint. Discussion started: 28 March 2023

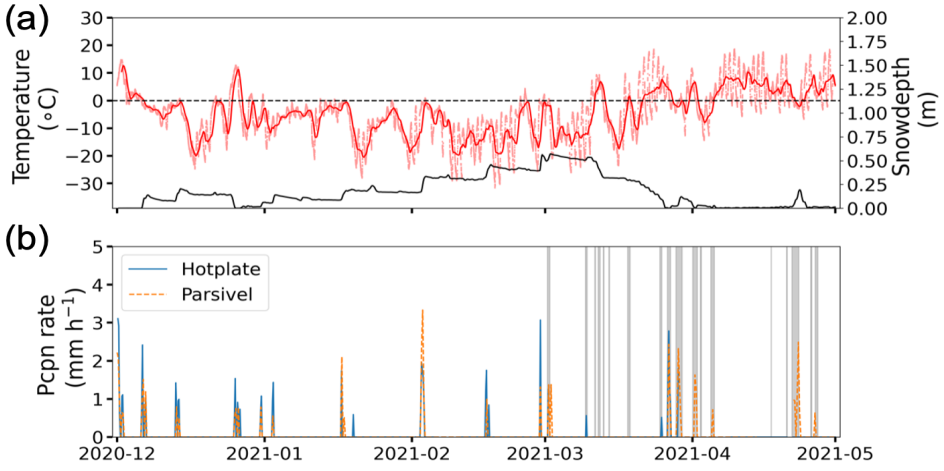

Figure 7: (a) Temperature and snow depth, and (b) precipitation measurements at the Fixed Station from December 2020 to April 2021. Red dashed line displays hourly temperature, solid red line represents 24 hour running mean. Snow depth (black line) is averaged over 24 hours. Precipitation rates (bottom) are averaged over 6 hours. No hotplate measurements are available, or therefore shown, for April due to an instrument fault. Grey vertical bands indicate periods of manual observations at the MUST Trailer during storm events by SAJESS volunteers and students.

4.3.2. Fixed Station storm measurements

Examples of the meteorological measurements at the fixed station are given Fig. 8. This example covers the period 25 – 27 December 2020 during which 22.5 hours of rain (1230 UTC 25 December – 1100 UTC 26 December), with temperatures of 5°C – 6°C, are followed closely by a decrease in temperature to < 0°C and ~4.5 hours of snow (1630 UTC – 2050 UTC 26 December 2021). Precipitation type derived by the fall speed and diameter measurements of the disdrometer correlated well with the change in air temperature. The MRR data show the reduction of melting height (determined by the sharp vertical gradient of reflectivity) from ~ 3 km AGL to just over ~ 2 km AGL during this same period.

https://doi.org/10.5194/essd-2023-59
Preprint. Discussion started: 28 March 2023

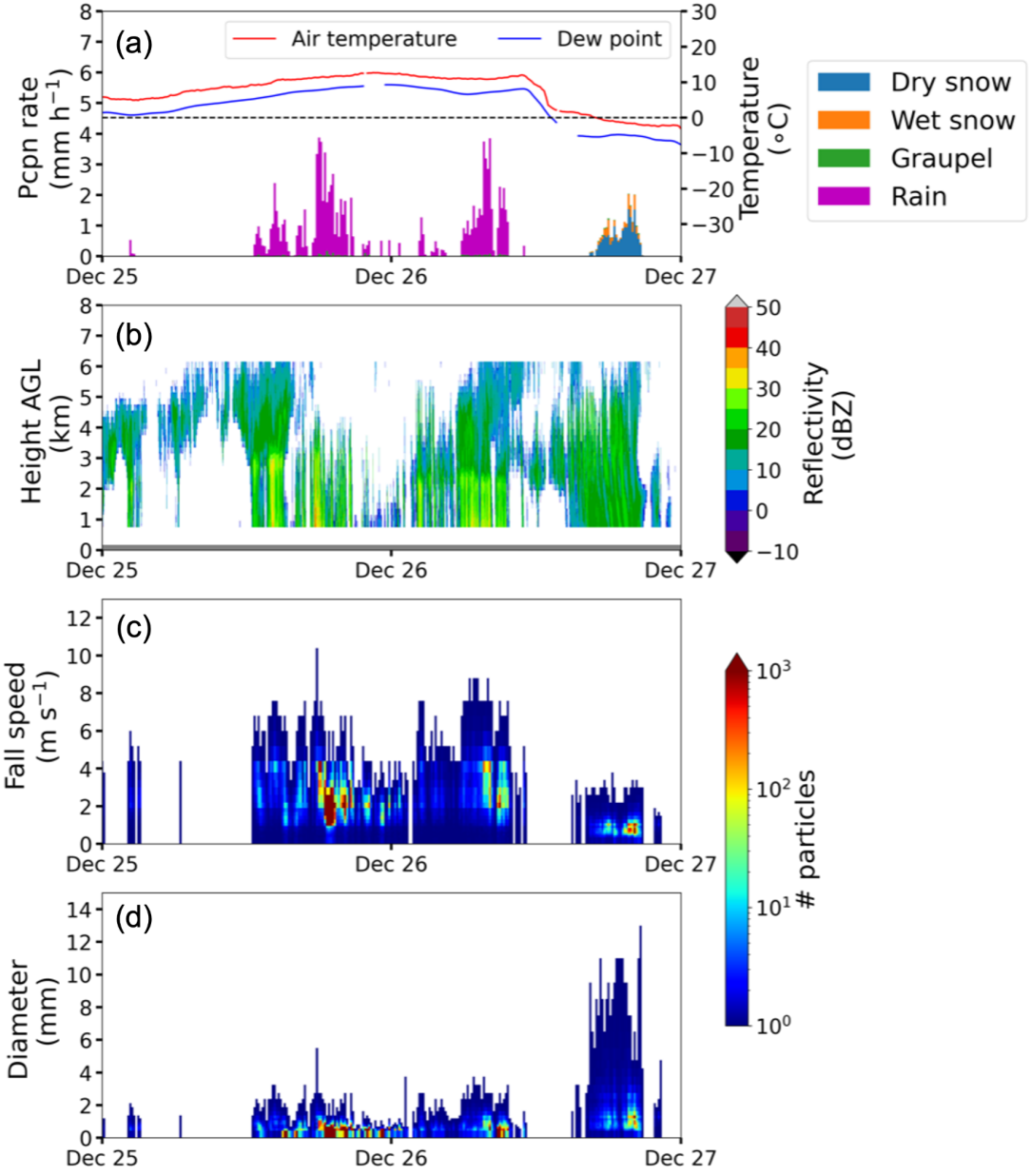

Figure 8: Fixed Station storm measurements. From top to bottom, (a) air temperature and precipitation, (b) radar reflectivity, (c) particle fallspeed, and (d) diameter (both from the Parsivel disdrometer), measured at the Fixed Station from 0000 UTC 25 December 2020 to 2359 UTC 26 December 2020. Temperature, dew point, precipitation, and disdrometer data are shown as 10-minute averages. Micro rain radar (MRR) data are at 10 second resolution, with a vertical resolution of 200 m.

https://doi.org/10.5194/essd-2023-59
Preprint. Discussion started: 28 March 2023

435

436 **4.3.3 MUST Station storm observations**

437 To complement the automated measurements made at the Fixed Station, the MUST Trailer site provided
438 observations of precipitation type, photographic imagery of particles, and upper air soundings. Images and
439 observations taken during a snow event that occurred on 18 March 2021 are shown in Figs. 9 and 10.

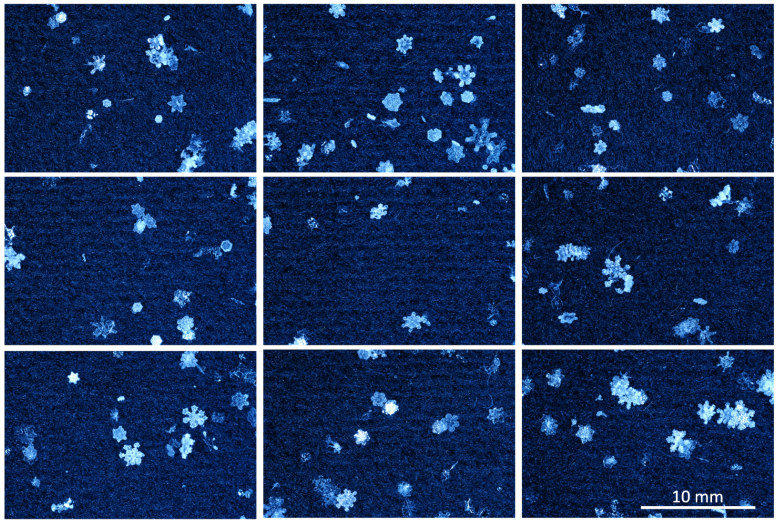

440

441 **Figure 9. MUST Trailer macrophotography. Nine independent (i.e., no overlap) images of the felt-covered pad with**
442 **solid hydrometeors collected at 1225 UTC 18 March 2021. Images are oriented as they were on the 13 cm × 13 cm pad.**

443

444 Macrophotography images taken from the SAJESS MUST Trailer provide confirmation of hydrometeor type.
445 When snow occurs, crystal habit, size distribution, and riming can be diagnosed. From 1000 UTC to 1430 UTC
446 18 March 2022, these images (Fig. 9), align with the 10-minute observations that recorded overcast skies,
447 nimbostratus clouds, and snow. Also, during this time, the MASC captured images of a variety of hydrometeors,
448 with the clearest images being of large aggregates (Fig. 10a). At 1200 UTC 18 March 2022 a deep saturated layer
449 between 900 and 700 hPa is evident on the upper air observations from the MUST Trailer, matching the vertical
450 profile observed in the National Weather Service (NWS) sounding from Caribou (ME) (Fig. 10b).

451

https://doi.org/10.5194/essd-2023-59
Preprint. Discussion started: 28 March 2023

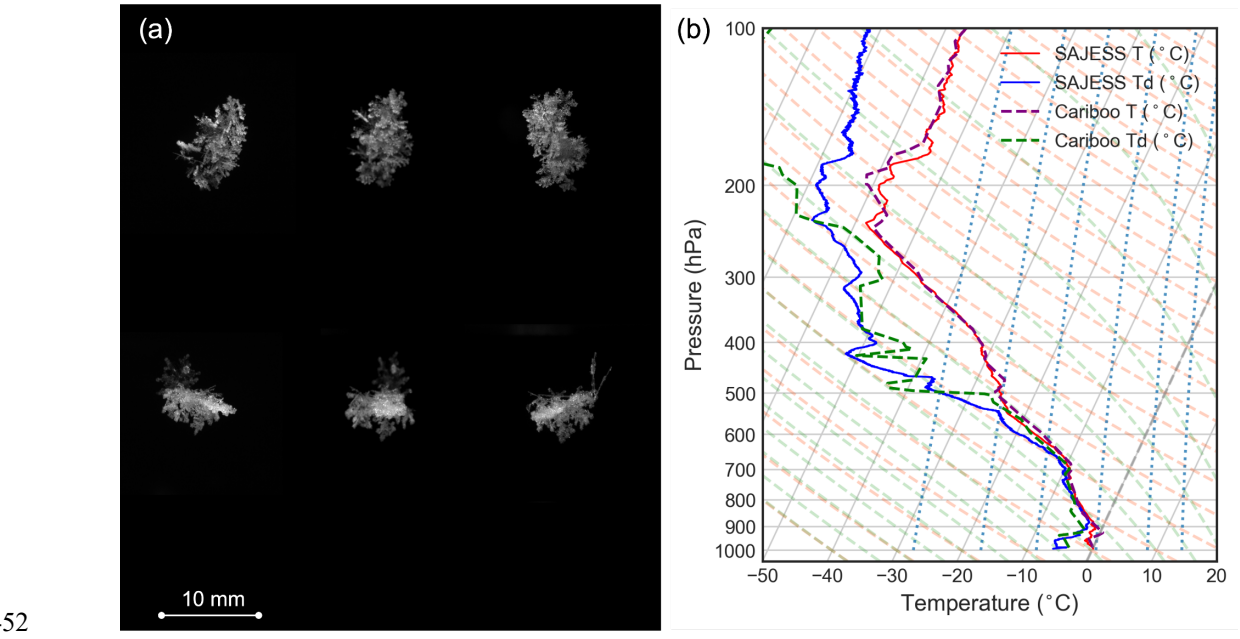

Figure 10. Multi-angle snowflake camera (MASC) images and upper air observations. (a) Two triplet images of aggregates taken by the MASC at 1240 UTC 18 March 2022, and (b) the 1200 UTC 18 March 2021 soundings from the SAJESS MUST Trailer and the NWS Caribou (ME) station.

4.4 Challenges and lessons-learned

Challenges during the SAJESS field campaign primarily originated from the requirement for remote computer access to monitor and troubleshoot instrument problems as they arose, and intermittent interruptions to AC power, especially at the Fixed Station site.

Such issues include the requirement to restart proprietary software. For example, the disdrometer software provided by OTT requires a user to restart the program manually if the computer has suffered a power interruption or reboot. This caused some periods of missing data to be longer than necessary. For subsequent deployments we have circumvented this issue by writing a serial-based terminal program in Python that can run on any operating system. Conversely, software provided by METEK for the MRR will restart automatically, however, users are limited to Windows operating software.

https://doi.org/10.5194/essd-2023-59
Preprint. Discussion started: 28 March 2023


Open Access Earth System Science Data Discussions

The processor included with the MRR Pro does allow for data collection to begin automatically, for as long as the on-board hard drive has space, however, raw data then are not retrievable as they are with the MRR2. We found this to be an adequate trade-off as the longer acquisition time per spectrum results in the MRR Pro signal having less noise, and due to the larger number of range gates, can have a finer vertical resolution for the same maximum height as the MRR2. Our use of both versions of the METEK MRR was also due to equipment limitations within the group.

A similar restart issue arose for the hotplate, whereby a manual reset was required after the instrument's microprocessor cut power to the heating plates. This response has been rectified by the manufacturer; however, we have since installed a remotely controlled AC outlet to our other hotplate stations that can be switched on/off without having to visit the site in-person.

SAJESS provided an opportunity to operate the multi-angle snowflake camera (MASC) during mixed-phased precipitation. Initial results indicate that the instrument can help diagnose mixed-phase precipitation using post-processing algorithms that diagnose particle fallspeed and diameter to a similar standard as the disdrometer. This leads, however, to many of the images being of blurred spherical raindrops rather than sharp pictures of ice crystal types published elsewhere. Work is ongoing to modify the post-processing software to include the categorization of raindrops, as this category is currently missing from the software.

Dishes for the SRS are required to be oriented to specific satellites (with the help of a satellite signal finder); however, it is also best if these dishes are not currently being used to receive a satellite TV signal by the household. In Edmundston, we located an adequate number of unused dishes within the community, however, an SRS specific deployment may require the purchasing of new equipment solely for the purpose of the SRS system. In some regions, satellite dishes may no longer be installed or maintained to a sufficient standard.

The use of community-based volunteers to assist in observations at times proved challenging, practically with respect to data quality. Our conclusion is that SAJESS could have benefited from a smaller number of high-quality measurements that could be verified, rather than a larger number of measurements that may have been prone to error. Due to public health measures in place much of the hands-on training that was planned had to be conducted remotely, and at times restrictions limited the volunteer's access to sites and equipment. We suggest a dedicated team member to act as liaison for larger groups of volunteers.

https://doi.org/10.5194/essd-2023-59
Preprint. Discussion started: 28 March 2023

Particularly difficult was the installation of the eddy covariance flux tripod during the winter season. The burial of temperature sensors and heat flux plates was less than ideal in the frozen surface material. However, care was taken to ensure restoration of the soil and turf was as complete as possible after installation. The overlying snow was also restored as homogeneously as possible to match the surrounding snowpack.

5 Summary

A valuable dataset was collected during the 2020-2021 Saint John River Experiment on Cold Season Storms (SAJESS) over Eastern Canada. The experiment led to a unique dataset to address precipitation amount and phase measurements at the surface and aloft across the upper Saint John River basin during one snowmelt season. Automatic measurements of precipitation and meteorological conditions at the surface and aloft were collected throughout the 2020-21 winter. Manual observations and augmented precipitation measurements were included during the intensive observations period from 8 March 2021 to 30 April 2021. Overall, data collected during SAJESS highlighted the need to enhance measurements of precipitation and snow in the upper Saint John River Basin to better anticipate ice jam and major flooding events along the Saint John River.

Author contributions

HDT wrote the first draft of the manuscript, as well as conducted some analyses. JMT, SJD, RES, and VV designed and led the field project. DB and LR collected manual observations during the intensive observational period. NDL contributed to the installation of the instruments and the management of the CoCoRaHS observers. MC provided the Smart Rainfall System (SRS). HDT, JMT, SJD, RES, DB, LR, NRL, MC and VV contributed to the writing and the editing of the manuscript.

Competing interests

The authors declare that they have no conflict of interest.

Data availability

https://doi.org/10.5194/essd-2023-59
Preprint. Discussion started: 28 March 2023

The SAJESS dataset (including the sample subset of data) is available from the Federated Research Data Repository (FRDR) and can be accessed at https://doi.org/10.20383/103.0591 (Thompson et al., 2023), and is included in the Global Water Futures FRDR collection. CoCoRaHS data are available from https://cocorahs.org/ViewData/. SRS data are available from the Artys' web platform (https:/www1.artys.it/) that can be accessed upon request (m.colli@artys.it).

Acknowledgments

Funding was provided by the Global Water Futures programme which is project 418474-1234 funded by the Canada First Research Excellence Fund, Natural Sciences and Engineering Research Council of Canada Discovery Grants (Julie M. Thériault, Stephen J. Déry, and Ronald E. Stewart), the Canada Research Chairs Program (Julie M. Thériault), and UNBC (Lisa Rickard), to conduct scientific analysis. The MUST Trailer was developed with funding from the Canadian Foundation for Innovation. Many thanks to all the volunteers and schools who collected measurements and provided locations fir the SRS parabolic dishes across northwest New Brunswick during SAJESS. Thank you to Jacques Doiron, Director of the Emergency Measures for the City of Edmundston, for providing the sites, facilities and coordinating the local activity with the SAJESS team, and Amanda Ronnquist for creating the SAJESS data management plan.

References

Angulo-Martínez, M., Beguería, S., Latorre, B., and Fernández-Raga, M.: Comparison of precipitation measurements by OTT Parsivel2 and Thies LPM optical disdrometers, Hydrological Earth System Science, 22, 2811–2837, https://doi.org/10.5194/hess-22-2811-2018, 2018.

Annandale, J., Jovanovic, N., Benadé, and N., Allen, R.: Software for missing data error analysis of Penman-Monteith reference evapotranspiration. Irrigation Science, 21, 57–67, https://doi.org/10.1007/s002710100047, 2002.

Apogee Instruments Inc.: Infrared radiometers owner's manual, https://www.apogeeinstruments.com/content/SI-400-manual.pdf, last access 9 March 2023, 2023.

https://doi.org/10.5194/essd-2023-59
Preprint. Discussion started: 28 March 2023

Beltaos, S., Ismail, S., and Burrell, B.: Midwinter breakup and jamming on the upper Saint John River: A case study, Canadian Journal of Civil Engineering, 30, 77-88, https://doi.org/10.1139/l02-062, 2011.

Buttle, J. M., Allen, D. M., Caissie, D., Davison, B., Hayashi, M., Peters, D. L., Pomeroy, J. W., Simonovic, S., St-Hilaire, A., and Whitfield, P. H.: Flood processes in Canada: Regional and special aspects, Canadian Water Resources Journal, 41(1–2), 7–30, https://doi.org/10.1080/07011784.2015.1131629, 2016.

Campbell Scientific (2022a): IRGASON: Integrated CO2 and H2O Open-Path Gas Analyzer and 3-D Sonic Anemometer. https://s.campbellsci.com/documents/us/manuals/irgason.pdf, last access: 31 August 2022, 20221a.

Campbell Scientific (2022b). EASYFLUX DL: EASYFLUX DL CR6OP or CR1KXOP For CR6 or CR1000X and Open-Path Eddy-Covariance Systems. Retrieved August 31, 2022, from https://s.campbellsci.com/documents/us/manuals/easyflux-dl-cr6op.pdf, last access: 31 August 2022, 2022b.

Cauteruccio, A., Chinchella, E., Stagnaro, M., and Lanza, L. G.: Snow particle collection efficiency and adjustment curves for the hotplate precipitation gauge. Journal of Hydrometeorology, 22(4), 941–954, https://doi.org/10.1175/JHM-D-20-0149.1, 2021.

Cifelli, R., Doesken, N., Kennedy, P., Carey, L. D., Rutledge, S. A., Gimmestad, C., and Depue, T.: The Community Collaborative Rain, Hail, and Snow Network: Informal education for scientists and citizens, Bulletin of the American Meteorological Society, 86(8), 1069–1077, http://www.jstor.org/stable/26221344, 2005.

Colli, M., Cassola, F., Martina, F., Trovatore, E., Delucchi, A., Maggiolo, S., and Caviglia, D.D.: Rainfall fields monitoring based on satellite microwave down-links and traditional techniques in the city of Genoa. IEEE Transactions on Geoscience Remote Sensing, 58(9), 6266–6280, https://doi.org/10.1109/TGRS.2020.2976137, 2020.

Colli, M., Stagnaro, M., Caridi, A., Lanza, L.G., Randazzo, A., Pastorino, M., Caviglia, D.D., and Delucchi, A.: A Field Assessment of a rain estimation system based on satellite-to-earth microwave links. IEEE Transactions on Geoscience Remote Sensing, 57(5), 2864–2875, https://doi.org/10.1109/TGRS.2018.2878338, 2019.

https://doi.org/10.5194/essd-2023-59
Preprint. Discussion started: 28 March 2023

589
590 Colorado Climate Center: Community collaborative rain, hail & snow network, CoCoRaHS Canada,
591 https://cocorahs.org/Canada.aspx, last access 15 March 2022, 2017.
592
593 Domine, F., Lackner, G., Sarrazin, D., Poirier, M., and Belke-Brea, M.: Meteorological, snow and soil data
594 (2013-2019) from a herb tundra permafrost site at Bylot Island, Canadian high Arctic, for driving and testing
595 snow and land surface models, Earth System Science Data, 13(9), 4331–4348. https://doi.org/10.5194/essd-13-
596 4331-2021, 2021.
597
598 Environment and Climate Change Canada: Top ten weather stories for 2008: story four: Saint John River floods
599 from top to bottom, https://www.ec.gc.ca/meteo-weather/default.asp?lang=En&n=7D6FDB7C-1, last access 25
600 March 2023, 2017.
601
602 Environment and Climate Change Canada: Canada's top 10 weather stories of 2018: 7. Flash flooding of the
603 Saint John River, https://www.canada.ca/en/environment-climate-change/services/top-ten-weather-
604 stories/2018.html#toc6, last access 25 March 2023, 2019.
605
606 Environment and Climate Change Canada: Canada's top 10 weather stories of 2019: 9. Saint John River floods
607 again. https://www.canada.ca/en/environment-climate-change/services/top-ten-weather-
608 stories/2019.html#toc10, last access 25 March 2023, 2020.
609
610 Falconi, M.T., von Lerber, A., Ori, D., Silvio Marzano, F., and Moisseev, D.: Snowfall retrieval at X, Ka and W
611 bands: consistency of backscattering and microphysical properties using BAECC ground-based measurements,
612 Atmospheric Measurement Techniques, 11, 3059-3079, https://doi.org/10.5194/amt-11-3059-2018, 2018.
613
614 Fitch, K. E., Hang, C., Talaei, A., and Garrett, T. J.: Arctic observations and numerical simulations of surface
615 wind effects on Multi-Angle Snowflake Camera measurement, Atmospheric Measurement Techniques, 14(2),
616 1127–1142. https://doi.org/10.5194/amt-14-1127-2021, 2021.
617

https://doi.org/10.5194/essd-2023-59
Preprint. Discussion started: 28 March 2023

618 Foken, T., Göockede, M., Mauder, M., Mahrt, L., Amiro, B., and Munger, W.: Post-Field Data Quality Control.
619 In: Lee, X., Massman, W., Law, B. (eds) Handbook of Micrometeorology, Atmospheric and Oceanographic
620 Sciences Library, vol 29, Springer, Dordrecht, https://doi.org/10.1007/1-4020-2265-4_9, 2004.
621
622 Fortin, G., and Dubreuil, V.: A geostatistical approach to create a new climate types map at regional scale: case
623 study of New Brunswick, Canada. Theoretical and Applied Climatology, 139(1–2), 323–334,
624 https://doi.org/10.1007/s00704-019-02961-2, 2020.
625
626 Garrett, T. J., Fallgatter, C., Shkurko, K., and Howlett, D.: Fall speed measurement and high-resolution multi-
627 angle photography of hydrometeors in free fall, Atmospheric Measurement Techniques, 5, 2625–2633,
628 https://doi.org/10.5194/amt-5-2625-2012, 2012.
629
630 Giannetti, F., and Reggiannini, R.: Opportunistic rain rate estimation from measurements of satellite downlink
631 attenuation: A survey. Sensors, 21(17), 5872, https://doi.org/10.3390/s21175872, 2021.
632
633 Gibson, S. R., and Stewart, R. E.: Observations of ice pellets during a winter storm. Atmospheric Research,
634 85(1), 64–76. https://doi.org/10.1016/j.atmosres.2006.11.004, 2007
635
636 Hicks, A., and Notaroš, B. M.: Method for classification of snowflakes based on images by a multi-angle
637 snowflake camera using convolutional neural networks. Journal of Atmospheric and Oceanic Technology,
638 36(12), 2267–2282, https://doi.org/10.1175/JTECH-D-19-0055.1, 2019.
639
640 Joe, P., Scott, B., Doyle, C., Isaac, G., Gultepe, I., Forsyth, D., Cober, S., Campos, E., Heckman, I., Donaldson,
641 N., Hudak, D., Rasmussen, R., Kucera, P., Stewart, R., Thériault, J. M., Fisico, T., Rasmussen, K. L.,
642 Carmichael, H., Laplante, A., … and Boudala, F.: The Monitoring network of the Vancouver 2010 Olympics,
643 Pure and Applied Geophysics, 171(1–2), 25–58, https://doi.org/10.1007/s00024-012-0588-z, 2014.
644
645 Kenny, J. L., and Secord, A. G.: Engineering modernity: Hydroelectric development in New Brunswick, 1945-
646 1970, Acadiensis, 39(1), 3–26, 2010.
647

Kochendorfer, J., Rasmussen, R., Wolff, M., Baker, B., Hall, M. E., Meyers, T., Landolt, S., Jachcik, A., Isaksen, K., Brækkan, R., and Leeper, R.: The quantification and correction of wind-induced precipitation measurement errors. Hydrology and Earth System Sciences, 21(4), 1973–1989, https://doi.org/10.5194/hess-21-1973-2017, 2017.

Liao, L., Meneghini, R., Tokay, A., and Bliven, L. F.: Retrieval of snow properties for Ku- and Ka-band dual-frequency radar, Journal of Applied Meteorology and Climatology, 55(9), 1845-1858, https://doi.org/10.1175/JAMC-D-15-0355.1, 2016.

Lapo, K. E., Hinkelman, L. M., Landry, C. C., Massmann, A. K., and Lundquist, J. D.: A simple algorithm for identifying periods of snow accumulation on a radiometer, Water Resoures. Research, 51, 7820– 7828, doi:10.1002/2015WR017590, 2015.

Maahn, M., and Kollias, P.: Improved Micro Rain Radar snow measurements using Doppler spectra post-processing. Atmospheric Measurement Techniques, 5(11), 2661–2673. https://doi.org/10.5194/amt-5-2661-2012, 2012.

METEK: MRR Physical Basics, 5.2.0.1, https://mpimet.mpg.de/fileadmin/atmosphaere/barbados/Instrumentation/MRR-physical-basics_20090707.pdf, last access: 25 March 2023, 2009.

METEK: Micro Rain Radar MRR-2, https://metek.de/wp-content/uploads/2014/05/Datasheet_MRR-2.pdf, last access 22 June 2022, 2010.

METEK: Micro Rain Radar MRR-PRO, https://metek.de/wp-content/uploads/2016/12/20180206_Datenblatt_MRR-PRO.pdf, last access 22 June 2022, 2017.

Newton, B., and Burrell, B. C.: The April–May 2008 flood event in the Saint John River Basin: Causes, assessment and damages. Canadian Water Resources Journal, 41(1–2), 118–128. https://doi.org/10.1080/07011784.2015.1009950, 2016.

https://doi.org/10.5194/essd-2023-59
Preprint. Discussion started: 28 March 2023

679 Nitu, R., Roulet, Y., Wolff, M., Earle, M., Reverdin, A., Smith, C., Kochendorfer, J., Morin, S., Rasmussen, R.,
680 Wong, K., Alastrué, J., Arnold, L., Baker, B., Buisan, S., Collado, J. L., Colli, M., Collins, B., Gaydos, A.,
681 Hannula, H.-R., … , and Senese, A.: WMO Solid Precipitation Intercomparison Experiment (SPICE) (2012-
682 2015), 131, World Meteorological Organization, 1429 pp.,
683 https://library.wmo.int/doc_num.php?explnum_id=5686, 2018.
684
685 Onset Computer Corporation: Hobo temperature/RH data logger, HOBO Temperature/RH Data Logger
686 MX2301A | Onset Data Loggers, https://www.onsetcomp.com/products/data-loggers/mx2301a/, last access 15
687 March 2022, 2022.
688
689 Pond Engineering: K63 Hotplate total precipitation gauge, http://www.pondengineering.com/k63, last access 25
690 March 2023, 2021.
691
692 Praz, C., Roulet, Y. A., and Berne, A.: Solid hydrometeor classification and riming degree estimation from
693 pictures collected with a Multi-Angle Snowflake Camera. Atmospheric Measurement Techniques, 10(4), 1335–
694 1357, https://doi.org/10.5194/amt-10-1335-2017, 2017.
695
696 Rasmussen, R. M., Hallett, J., Purcell, R., Landolt, S. D., and Cole, J.: The hotplate precipitation gauge, Journal
697 of Atmospheric and Oceanic Technology, 28(2), 148–164, https://doi.org/10.1175/2010JTECHA1375.1, 2011.
698
699 Raupach, T. H., and Berne, A.: Correction of raindrop size distributions measured by Parsivel disdrometers,
700 using a two-dimensional video disdrometer as a reference, Atmospheric Measurement Techniques, 8(1), 343–
701 365. https://doi.org/10.5194/amt-8-343-2015, 2015.
702
703 Schaer, M., Praz, C., and Berne, A.: Identification of blowing snow particles in images from a Multi-Angle
704 Snowflake Camera. Cryosphere, 14(1), 367–384, https://doi.org/10.5194/tc-14-367-2020, 2020.
705
706 Sicart, J.E., Pomeroy, J.W., Essery, R.L.H. and Bewley, D.: Incoming longwave radiation to melting snow:
707 observations, sensitivity and estimation in Northern environments, Hydrological Processes, 20, 3697-3708,
708 https://doi.org/10.1002/hyp.6383, 2006.
709

https://doi.org/10.5194/essd-2023-59
Preprint. Discussion started: 28 March 2023

710 Skofronick-Jackson, G., Hudak, D., Petersen, W., Nesbitt, S. W., Chandrasekar, V., Durden, S., Gleicher, K. J.,
711 Huang, G. J., Joe, P., Kollias, P., Reed, K. A., Schwaller, M. R., Stewart, R., Tanelli, S., Tokay, A., Wang, J. R.,
712 and Wolde, M.: Global precipitation measurement cold season precipitation experiment (GCPEX): For
713 measurement's sake, let it snow, Bulletin of the American Meteorological Society, 96(10), 1719–1741,
714 https://doi.org/10.1175/BAMS-D-13-00262.1, 2015.
715
716 Souverijns, N., Gossart, A., Lhermitte, S., Gorodetskaya, I. V., Kneifel, S., Maahn, M., Bliven, F. L., & van
717 Lipzig, N. P. M. (2017). Estimating radar reflectivity - Snowfall rate relationships and their uncertainties over
718 Antarctica by combining disdrometer and radar observations. Atmospheric Research, 196(June), 211–223.
719 https://doi.org/10.1016/j.atmosres.2017.06.001
720
721 Thériault, J. M., Hung, I., Vaquer, P., Stewart, R. E., and Pomeroy, J.: Precipitation characteristics and
722 associated weather conditions on the eastern slopes of the Rocky Mountains during March and April 2015l,
723 Hydrology and Earth System Sciences, 22(8), 4491–4512, https://doi.org/10.5194/hess-22-4491-2018, 2018.
724
725 Thériault, J. M., Déry, S. J., Pomeroy, J. W., Smith, H. M., Almonte, J., Bertoncini, A., Crawford, R. W.,
726 Desroches-Lapointe, A., Lachapelle, M., Mariani, Z., Mitchell, S., Morris, J. E., Hébert-Pinard, C., Rodriguez,
727 P., and Thompson, H. D.: Meteorological observations collected during the Storms and Precipitation across the
728 continental Divide Experiment (SPADE), April-June 2019, Earth System Science Data, 13(3), 1233–1249,
729 https://doi.org/10.5194/essd-13-1233-2021, 2021a.
730
731 Thériault, J. M., Leroux, N. R., and Rasmussen, R. M.: Improvement of solid precipitation measurements using
732 a hotplate precipitation gauge, Journal of Hydrometeorology, 22(4), 877–885, https://doi.org/10.1175/JHM-D-
733 20-0168.1, 2021b.
734
735 Thompson, H. D., Thériault, J. M., Déry, S. J., Stewart, R. E., Boisvert, D., Rickard, L., Leroux, N. R., Colli,
736 M., and Vincent Vionnet, V.: Atmospheric and surface observation data collected during the Saint John River
737 Experiment on Cold Season Storms, Federated Research Data Repository [data set],
738 https://doi.org/10.20383/103.059, 2023.
739

https://doi.org/10.5194/essd-2023-59
Preprint. Discussion started: 28 March 2023

740 Tokay, A., Hartmann, P., Battaglia, A., Gage, K. S., Clark, W. L., and Williams, C. R.: A field study of
741 reflectivity and Z-R relations using vertically pointing radars and disdrometers, Journal of Atmospheric and
742 Oceanic Technology, 26(6), 1120–1134, https://doi.org/10.1175/2008JTECHA1163.1, 2009.
743
744 US Department of Energy: Toolbox — A rolling list of software/packages for flux-related data processing,
745 FLUXNET: The Data Portal Serving the FLUXNET Community, https://fluxnet.org/2017/10/10/toolbox-a-
746 rolling-list-of-softwarepackages-for-flux-related-data-processing/, last access 31 August 2022, 2021.

https://doi.org/10.5194/essd-2023-59
Preprint. Discussion started: 28 March 2023

Table 1. Primary site information

Location	Lat (°N)	Lon (°W)	Elevation (m)	Surface	Surroundings	Dates of operation for SAJESS
Fixed Station	47.418	68.324	152	Grassland on gravel riverbed	Open grassland in broad river valley, rural road ~150 m to the west	1 December 2020 – 30 April 2021
MUST Trailer	47.361	68.320	143	Packed gravel, short grass	Site on edge of city treatment ponds, ~ 250 m from confluence of two large rivers; suburban subdivision to the north,	1 March 2021 – 30 April 2021

https://doi.org/10.5194/essd-2023-59
Preprint. Discussion started: 28 March 2023

Table 2. Instrument details for the SAJESS Fixed Station site

Installation (instrument abbr.)	Instrument	Installation height	Variable	Units	Resolution	Accuracy
Met tripod (MET)	Campbell Scientific CR1000X datalogger	1.5 m	data recording	NA	NA	NA
	OTT Parsivel^2 disdrometer	2.80 m	Particle fall speed Particle diameter	m s^{-1} mm	1 min (average)	±1 size class (0.2 to 2 mm) ±0.5 size class (>2mm)
	Vaisala HMP155 temperature/RH probe	2.00 m	Air temperature Relative Humidity	°C %	1 min (average)	0.226+0.0028×reading (−80 to +20 °C) 0.055+0.0057×reading (+20 to +60 °C)
	Kipp & Zonen CNR4 Net radiometer	1.80 m	4-way net radiation	W m^{-2}	1 min (average)	< 5 %
	Campbell Scientific SR50A sonic ranger	1.80 m	Snow depth	m	1 min (average)	±1 cm
	Apogee SI-411 IR radiometer	1.80 m	Surface temperature	°C	1 min (average)	±0.2 °C
	Campbell Scientific CS655 Soil probe (vertically)	0.00 m	Soil temperature Soil moisture content Soil electrical conductivity	°C % dS m^{-1}	1 min (average)	±0.1 - 0.5 °C ±1 - 3% ±5% of reading + 0.05 dS m^{-1}
MRR tripod (MRR)	METEK MRR-2	2.60 m	Doppler raw spectra Reflectivity (Ze) Doppler velocity (W) Spectral width (σ)	dB dBz m s^{-1} m s^{-1}	10 sec raw data; 1 min average	0.53 dB 0.53 dBZ 0.109 ms^{-1} 0.09 ms^{-1}
Hotplate tripod (HP)	Pond engineering K63 Hotplate precipitation gauge	2.60 m	Air temperature Barometric pressure Precipitation rate Accumulation Windspeed Hotplate power	°C kPa mm hr^{-1} mm m s^{-1} W	1 min (average) 5 min (average)	±1 °C ±1 kPa ±0.5 mm hr^{-1} ±0.5 mm ±1 ms^{-1} NA
Flux tripod (FLUX)	Campbell Scientific CR1000X datalogger	1.5 m	data recording	NA	NA	NA
	Vaisala HMP155 Temperature/RH probe	2.00 m	Air temperature Relative humidity	°C %	30 min (average)	0.226+0.0028×reading (−80 to +20 °C) 0.055+0.0057×reading (+20 to +60 °C)
	Apogee SI-411 Infrared radiometer	1.80 m	Surface temperature	°C	30 min (average)	±0.2 °C

https://doi.org/10.5194/essd-2023-59
Preprint. Discussion started: 28 March 2023

	Kipp & Zonen CNR4 Net radiometer	1.80 m	4-way net radiation	W m^{-2}	30 min (average)	< 5 %
	Campbell Scientific IRGASON	2.00 m	3D wind CO2 density H20 density Sonic temperature	m s^{-1} mg·m^{-3} g·m^{-3} °C	10 Hz	1 mm s-1 0.2 mg·m^{-3} (0.15 µmol·mol^{-1}) 0.00350 g·m^{-3} (0.006 mmol·mol^{-1}) 0.025 °C
	Campbell Scientific CS655 Soil probe	2.5 cm below surface	Soil temperature Soil moisture content Soil electrical conductivity	°C % dS m^{-1}	30 min (average)	±0.1 - 0.5 °C ±1 - 3% ±5% of reading + 0.05 dS m^{-1}
	Campbell Scientific HFP01 Soil heat flux plates	8 cm below surface	Soil heat flux	W m^{-2}	30 min (average)	-15% to +5% in most common soils

https://doi.org/10.5194/essd-2023-59
Preprint. Discussion started: 28 March 2023

Table 3. Instrument details for the SAJESS MUST Trailer site

Installation (Instrument abbr.)	Instrument	Installation height	Variable	Units	Resolution	Accuracy
Met tripod (MET)	Campbell Scientific CR1000X datalogger	1.5 m	data recording	NA	NA	NA
	Vaisala HMP155 Temperature/RH probe	2.00 m	Air temperature Relative humidity	°C %	1 min (average)	0.226+0.0028×reading (−80 to +20 °C) 0.055+0.0057×reading (+20 to +60 °C)
	Kipp & Zonen CNR4 Net radiometer	1.80 m	Net 4-way radiation	W m^{-2}	1 min (average)	< 5 %
	Campbell Scientific SR50A	1.80 m	Snow depth	m	1 min (average)	±1 cm
10 m Mast (MAST)	Campbell Scientific CR1000X datalogger	1.5 m	data recording	NA	NA	NA
	Pond engineering K63 Hotplate precipitation gauge	2.60 m	Air temperature Barometric pressure Precipitation rate Accumulation Windspeed Hotplate power	°C kPa mm hr^{-1} mm m s^{-1} W	1 min (average) 5 min (average)	±1 °C ±1 kPa ±0.5 mm hr^{-1} ±0.5 mm ±1 ms^{-1} NA
	RM Young 05103AP alpine wind monitor	10.0 m	Wind speed Wind direction	m s^{-1} degrees	1 min (average)	± 0.3 m s^{-1} ± 5 degrees
MASC Platform (MASC)	Multi-angle snowflake camera	1.00 m	Series of 3 images	NA	Up to 3 Hz	NA
MRR Pro (MRR)	METEK MRR Pro	1.30.m	Doppler raw spectra Reflectivity (Ze) Doppler velocity (*W*) Spectral width (σ)	dB dBz m s^{-1} m s^{-1}	30 sec (average)	0.53 dB 0.53 dBZ 0.109 ms^{-1} 0.09 ms^{-1}
Macrophotography (MP)	Nikon D80 with 60 mm macro lens	NA	Series of 9 images	N/A	10 min	NA
Manual observations (OBS)	Volunteer and/or student	NA	Sky condition Cloud type Precipitation type Blowing snow Light precipitation	Oktas Type Type Y/N Y/N	10 min	NA
Upper air observations	iMet-3050A 403 MHz portable sounding	NA	Air temperature Relative humidity	°C %	1 sec	± 0.5 - 1.0 °C ± 5%

https://doi.org/10.5194/essd-2023-59
Preprint. Discussion started: 28 March 2023

(SB)	system with iMet-4 radiosonde		Wind speed	$m\ s^{-1}$		$\pm$ 0.5 $m\ s^{-1}$
			Wind direction	degrees		$\pm$ 1 degrees
			Pressure	hPa		$\pm$ 0.5 - 2.0 hPa
			Geopotential height	m		$\pm$ 15 m

'57

https://doi.org/10.5194/essd-2023-59
Preprint. Discussion started: 28 March 2023

Table 4. Location of each HOBO MX2301A data logger, including the corresponding CoCoRaHS ID (if applicable)

Temperature sensor ID (serial number)	CoCoRaHS ID	Lat (°N)	Lon (°W)	Elevation (m)	Period of Record
SJ_HOBOTEMP_01 (20816232)	CAN-NB-111	47.37	68.32	166	11 December 2020 - 30 April 2021
SJ_HOBOTEMP_02 (20816241)	CAN-NB-113	47.25	68.03	155	11 December 2020 - 30 April 2021
SJ_HOBOTEMP_03 (20816231)	CAN-NB-114	47.37	68.31	197	10 December 2020 - 30 April 2021
SJ_HOBOTEMP_04 (20816166)	CAN-NB-115	47.43	68.39	142	10 December 2020 - 30 April 2021
SJ_HOBOTEMP_05 (20816234)	CAN-NB-117	47.45	68.32	326	11 December 2020 - 30 April 2021
SJ_HOBOTEMP_06 (20186244)	CAN-NB-127	47.36	68.16	176	5 March 2021 - 30 April 2021
SJ_HOBOTEMP_07 (20689495)	CAN-NB-133	47.35	68.46	332	5 March 2021 - 30 April 2021
SJ_HOBOTEMP_08 (20816235)	CAN-NB-135	47.26	68.61	167	12 December 2020 - 30 April 2021
SJ_HOBOTEMP_09 (20816239)	CAN-NB-139	47.37	68.34	241	10 December 2020 - 30 April 2021
SJ_HOBOTEMP_10 (20816242)	CAN-NB-143	47.24	68.70	170	12 December 2020 - 30 April 2021
SJ_HOBOTEMP_11 (20816245)	CAN-NB-144	47.37	68.28	141	10 December 2020 - 30 April 2021
SJ_HOBOTEMP_12 (20816233)	CAN-NB-145	47.33	68.09	231	5 March 2020 - 30 April 2021
SJ_HOBOTEMP_13 (20689496)	N/A	47.29	68.39	156	5 March 2021 - 30 April 2021